Calculation of bound and resonance states of HO 2 for nonzero total angular momentum

Hong Zhang and Sean C. Smith

Citation: The Journal of Chemical Physics **118**, 10042 (2003); doi: 10.1063/1.1572132
View online: http://dx.doi.org/10.1063/1.1572132
View Table of Contents: http://scitation.aip.org/content/aip/journal/jcp/118/22?ver=pdfcov
Published by the AIP Publishing

Calculation of bound and resonance states of HO_2 for nonzero total angular momentum

Hong Zhang and Sean C. Smith[a)]
Centre for Computational Molecular Science, Chemistry Building 68, The University of Queensland, Qld 4072, Brisbane, Australia

(Received 28 January 2003; accepted 14 March 2003)

Bound and resonance states of HO_2 have been calculated quantum mechanically by the Lanczos homogeneous filter diagonalization method [Zhang and Smith, Phys. Chem. Chem. Phys. **3**, 2282 (2001); J. Chem. Phys. **115**, 5751 (2001)] for nonzero total angular momentum $J=1,2,3$. For lower bound states, agreement between the results in this paper and previous work is quite satisfactory; while for high lying bound states and resonances these are the first reported results. A helicity quantum number Ω assignment (within the helicity conserving approximation) is performed and the results indicate that for lower bound states it is possible to assign the Ω quantum numbers unambiguously, but for resonances it is impossible to assign the Ω helicity quantum numbers due to strong mixing. In fact, for the high-lying bound states, the mixing has already appeared. These results indicate that the helicity conserving approximation is not good for the resonance state calculations and exact quantum calculations are needed to accurately describe the reaction dynamics for HO_2 system. Analysis of the resonance widths shows that most of the resonances are overlapping and the interferences between them lead to large fluctuations from one resonance to another. In accord with the conclusions from earlier $J=0$ calculations, this indicates that the dissociation of HO_2 is essentially irregular. © *2003 American Institute of Physics.*
[DOI: 10.1063/1.1572132]

I. INTRODUCTION

Resonances are temporarily trapped meta-stable states, which are formed by bound-free excitations or by collisions between reactants. After some finite time they will decay into products. In essence, resonances are quantum mechanical phenomena because they occur at discrete energies (resonance positions), but unlike bound states they have a finite width (resonance width). Resonances are more difficult to characterize computationally than bound states, not only because of the progressive increase in computational demands as one moves up into denser regions of the spectrum, but also because of the nonlocalization of their wave functions (extending to infinity). Though long recognized in the literature, the quantitative determination of resonances started to appear only during past two decades for triatomic systems. There are basically two ways to determine the resonance energies and widths. The first one can be described as the boundlike eigenvalue problem. In this method, the resonance positions and widths are, respectively, associated with the real and imaginary part of the complex eigenvalues of the absorbing potential augmented Hamiltonian[1–6] or complex scaled Hamiltonian.[7–10] The second one is the so-called scattering method, which rely on the scattering S matrix calculations.[11–13] Resonance states are associated with the complex poles of the S matrix and thus all S matrix related quantities such as lifetime matrix or scattering probabilities will reflect the resonance structures in their energy dependent profiles. Analysis of the profiles can lead to resonance energies as well as widths.

Resonances can be generally classified into three categories according to the shapes of the potential energy surfaces (PES), namely, unbound, weakly bound, and strongly bound systems. Three typical examples are, respectively, $H+H_2$, HCO, and HO_2 (or their isotopes), which have been extensively investigated both theoretically and experimentally, and several review articles have appeared over the past decades.[14–23] Among the three types of resonances, complex forming systems are more difficult to compute. This is because the PES generally has a deep well supporting a dense spectrum and thus more iterations are needed in time-independent (TI) quantum iterative methods, or alternatively more time is needed in time-dependent (TD) wave packet methods. The potential well on the ground state PES of HO_2 is 2.38 eV deep, supporting over 350 bound states of odd exchange parity (for $J=0$). It therefore has a relatively high density of states, making this system a very complicated and challenging one to characterize. For this system, there have been several reports of total angular momentum $J=0$ bound and resonance calculations.[13,24–33] There is only one report of calculations of the low-lying bound states for small nonzero J values,[34] and no reports of resonance calculations for nonzero J. There have been several reports detailing calculations of the initial-state-resolved reaction probability for $H+O_2$ reaction.[29,30,35–43] While most of the calculations focus on $J=0$, $J>0$ total reaction probability calculations have appeared in recent rears.[39–41] These $J>0$ calculations focus

a)Author to whom correspondence should be addressed. Fax: 61-7-3365-4623. Electronic mail: s.smith@uq.edu.au

mainly on the total angular momentum dependence of the global shape of the reaction probabilities and of the mechanisms governing the reaction, and the details of the individual resonances are not considered. In particular, there are no reported calculations focusing on the energy region in which only one arrangement channel is open, i.e., above the first reaction threshold and below the second reaction threshold, which is the main focus in this paper. The continuing interest in the HO_2 system is motivated not only by its importance as a benchmark system for computational methods, but also by its importance in combustion and atmospheric chemistry.[44]

Exact $J>0$ calculations are essential in fully understanding quantum reaction dynamics. For example, in unimolecular dissociation, to understand the temperature variation of rate constants, it is important to implement $J>0$ calculations as accurately as possible. In bimolecular reactions, the detailed cross sections can only be obtained after summing over many manifolds of scattering matrix elements associated with nonzero J. However, these $J>0$ calculations are still very challenging even for triatomic reactions, especially when dealing with complex-forming systems. The major reason for this situation is the so-called ''angular momentum catastrophe:'' [45] many $J>0$ calculations have to be performed, and the size of the Hamiltonian matrix increases linearly with J. Thus approximate quantum methods such as adiabatic rotation,[46] J-shifting,[47] and helicity conserving (HC)[48] approximations are commonly used. As important as exact quantum methods may be, approximations may become unavoidable for complex or/and large systems. However, for the complex forming reaction such as HO_2, it seems that the Coriolis coupling is important due to its floppiness, and these approximations might cause some inaccuracies, even errors. In another word, is there a reasonably good quantum number Ω associated with the projection of total angular momentum on a body fixed axis? If the substates Ω of the wave function for $J>0$ are heavily coupled, the Coriolis coupling between the states cannot be ignored and any attempts to assign the helicity quantum number Ω will fail. We will examine this issue by a helicity quantum number Ω assignment for both bound and resonance states. If this assignment is successful, the approximate helicity conserving calculations may be applied, otherwise the Coriolis coupling should not be ignored and exact quantum methods have to be used.

For exact quantum methods, there are several representations which can be utilized, such as close-coupled representations (CCR),[49] finite basis representations (FBR), discrete variable representations (DVR),[50] and pseudo-spectral transformation representations (PSTR).[51,52] These representations are closely related, and each has its advantages as well as its disadvantages. In this paper we will use a DVR for the internal Jacobi coordinates. The advantage of DVRs is that the potential matrix is diagonal, which will reduce the memory requirement substantially. For the three Eulerian angles we employ a FBR. After setting up the Hamiltonian matrix, one can use iterative methods such as standard complex symmetric Lanczos method[53,54] to calculate the eigenvalues. However, Lanczos subspace filter diagonalization (LSFD) methods[24,25,32,33,55–57] recently developed in this group may have many advantages over the standard Lanczos method. First, LSFD is more efficient than standard Lanczos method because only a small sized generalized eigenproblem needs to be solved in LSFD. It is relatively easy to set up the small eigen-problem since representing the Hamiltonian tridiagonally makes it a straightforward exercise to generate a set of filtered states for each energy window within the Lanczos subspace. For challenging molecular applications the rank of the tridiagonal representation of $\hat{H}$ can typically be in the range of 10^4-10^6, in which case the diagonalization to extract eigenvalues using standard Lanczos method can consume significant amounts of cpu time (not to mention many additional diagonalisations used for convergence checking as the size of the Lanczos basis increases). LSFD is especially useful when one only considers a small section of the entire spectrum as in most applications. In addition, LSFD has the desirable property of avoiding most of the ghost eigenvalues that will appear in standard Lanczos diagonalization. Different Lanczos FD versions have been proposed such as quasiminimum residual (QMR) FD or minimum residual (MINRES) FD approaches.[33,55,56] Very recently we have developed a simpler and more efficient Lanczos homogeneous filter diagonalization (LHFD) algorithm based on a very simple homogeneous filtering recursion within the Lanczos representation.[24,25] This LHFD method has been employed on $J=0$ bound and resonance state calculations for HO_2 system.[24] In this report, we will extend the LHFD method into exact $J>0$ calculations for this system for $J=1,2,3$.

The rest of this article is organized as follows: In Sec. II we describe the theoretical methods needed to characterize both bound and resonance states for nonzero total angular momentum. In Sec. III we shall give some computational details and present the results of $J>0$ bound and resonance calculations performed on the HO_2 system. Section IV concludes.

II. THEORETICAL METHODS

A. Hamiltonian

In general, we treat the three internal Jacobi coordinates (R,r,γ) on discrete grids, while the three Eulerian angles (θ, ϕ, ψ) are described in a basis set. This procedure is very efficient because the potential part of the Hamiltonian matrix is diagonal, which can reduce the memory requirement substantially. The following presentations follow the basic definitions, and our purpose is to reduce the 6D Hamiltonian into a 4D tridiagonal block matrix for each single J value. Here we do not give more details, and for that purpose the reader is referred to earlier works.[58–60]

The triatomic Hamiltonian in Jacobi coordinates for HO_2 system in body fixed frame is given by

$$\hat{H}=-\frac{\hbar^2}{2\mu}\frac{1}{R}\frac{\partial^2}{\partial R^2}R-\frac{\hbar^2}{2\mu}\frac{1}{r}\frac{\partial^2}{\partial r^2}r+\frac{\hat{l}^2}{2\mu R^2}+\frac{\hat{j}^2}{2\mu r^2}+V(R,r,\gamma), \tag{1}$$

where orbital angular momentum $\hat{l}^2=(\hat{J}-\hat{j})^2=\hat{J}^2+\hat{j}^2-2\hat{J}\cdot\hat{j}$. Expressing the angular momentum parts of the Hamiltonian explicitly,

$$\hat{J}^2=-\hbar^2\left[\frac{\partial^2}{\partial\theta^2}+\cot\theta\frac{\partial}{\partial\theta}+\frac{1}{\sin^2\theta}\left(\frac{\partial^2}{\partial\phi^2}+\frac{\partial^2}{\partial\psi^2}\right)-\frac{2\cos\theta}{\sin^2\theta}\frac{\partial^2}{\partial\phi\,\partial\psi}\right], \tag{2}$$

$$\hat{j}^2=-\hbar^2\left(\frac{\partial^2}{\partial\gamma^2}+\cot\gamma\frac{\partial}{\partial\gamma}+\frac{1}{\sin^2\gamma}\frac{\partial^2}{\partial\psi^2}\right), \tag{3}$$

$$\hat{J}\cdot\hat{j}=-\hbar^2\left[\begin{array}{l}-\sin\psi\cot\gamma\dfrac{\partial^2}{\partial\psi\,\partial\theta}+\cos\psi\dfrac{\partial^2}{\partial\gamma\,\partial\theta}+(1-\cos\psi\cot\gamma\cot\theta)\dfrac{\partial^2}{\partial\psi^2}\\ \quad+\dfrac{\cos\psi\cot\gamma}{\sin\theta}\dfrac{\partial^2}{\partial\psi\,\partial\phi}+\dfrac{\sin\psi}{\sin\theta}\dfrac{\partial^2}{\partial\gamma\,\partial\phi}-\sin\psi\cot\theta\dfrac{\partial^2}{\partial\psi\,\partial\gamma}\end{array}\right], \tag{4}$$

and using symmetry-adapted symmetric top eigenfunctions to expand the total wave function, one can get the coupled equations,

$$\begin{aligned}\hat{H}_{\Omega,\Omega}=&-\frac{\hbar^2}{2\mu}\frac{1}{R}\frac{\partial^2}{\partial R^2}R-\frac{\hbar^2}{2\mu}\frac{1}{r}\frac{\partial^2}{\partial r^2}r+V(R,r,\gamma)\\&+\left(\frac{1}{2\mu R^2}+\frac{1}{2\mu r^2}\right)\left(-\frac{\hbar^2}{\sin\gamma}\frac{\partial}{\partial\gamma}\sin\gamma\frac{\partial}{\partial\gamma}+\frac{\hbar^2\Omega^2}{\sin^2\gamma}\right)\\&+\frac{\hbar^2}{2\mu R^2}[J(J+1)-2\Omega^2]\end{aligned} \tag{5}$$

and

$$\begin{aligned}\hat{H}_{\Omega,\Omega\pm1}=&(1+\delta_{\Omega,m})^{1/2}\frac{\hbar^2}{2\mu R^2}\sqrt{J(J+1)-\Omega(\Omega\pm1)}\\&\times\left[\pm\frac{\partial}{\partial\gamma}+(\Omega\pm1)\cot\gamma\right],\end{aligned} \tag{6}$$

with $m=0$ for $\hat{H}_{\Omega,\Omega+1}$ and $m=1$ for $\hat{H}_{\Omega,\Omega-1}$. Such coupled equations can be represented in any one of the four representations mentioned above. In our calculations, we use DVR:

$$\begin{aligned}H^{\lambda'\Omega'}_{\lambda\Omega}=&-\frac{\hbar^2}{2\mu}\frac{1}{R}\frac{\partial^2}{\partial R^2}R\delta_{\lambda'\lambda}\delta_{\Omega'\Omega}-\frac{\hbar^2}{2\mu}\frac{1}{r}\frac{\partial^2}{\partial r^2}r\delta_{\lambda'\lambda}\delta_{\Omega'\Omega}+V(R,r,\gamma^{\Omega}_{\lambda})\delta_{\Omega'\Omega}+\left(\frac{1}{2\mu R^2}+\frac{1}{2\mu r^2}\right)\\&\times\sum_j T^{\Omega}_{j\lambda}[j(j+1)\hbar^2]T^{\Omega}_{j\lambda'}\delta_{\Omega'\Omega}+\frac{\hbar^2}{2\mu R^2}[J(J+1)-2\Omega^2]\delta_{\lambda'\lambda}\delta_{\Omega'\Omega}\\&+\sum_j T^{\Omega}_{j\lambda}t^{Jj}_{\Omega,\Omega+1}T^{\Omega+1}_{j\lambda'}\delta_{\Omega'\Omega+1}+\sum_j T^{\Omega}_{j\lambda}t^{Jj}_{\Omega,\Omega-1}T^{\Omega-1}_{j\lambda'}\delta_{\Omega'\Omega-1},\end{aligned} \tag{7}$$

with

$$t^{Jj}_{\Omega,\Omega\pm1}=-(1+\delta_{\Omega,m})^{1/2}\frac{\hbar^2}{2\mu R^2}\sqrt{J(J+1)-\Omega(\Omega\pm1)}\sqrt{j(j+1)-\Omega(\Omega\pm1)}.$$

In Eq. (7), we have used Ω-dependent DVR for γ coordinate, which is obtained by either diagonalizing the coordinate operator ($x=\cos\gamma$) matrix ${}^{\Omega,\gamma}\Delta_{jj'}=\int^1_{-1}\Theta^{\Omega}_j(\gamma)x\Theta^{\Omega}_{j'}(\gamma)dx$ or by a Gauss-Jacobi quadrature scheme ${}^{\Omega,\gamma}\Delta_{jj'}=\int^1_{-1}W(x)\tilde{\Theta}^{\Omega}_j(\gamma)x\tilde{\Theta}^{\Omega}_{j'}(\gamma)dx$. Here $\Theta^{\Omega}_j(\gamma)$ is the associated Legendre polynomial, the weight function $W(x)=(1-x^2)^{\Omega}$, and $\tilde{\Theta}^{\Omega}_j(\gamma)=\Theta^{\Omega}_j(\gamma)/\sqrt{(1-x^2)^{\Omega}}$. In Gauss–Jacobi quadrature scheme, the transformation matrix is set up according to $T^{\Omega}_{j\lambda}=\sqrt{\omega_\lambda}\tilde{\Theta}^{\Omega}_j(x_\lambda)$. Here λ is used to label the DVR in the γ coordinate, and x_λ and ω_λ are the quadrature points and weights, respectively, which can be obtained from standard methods.[61] In a direct diagonalization scheme, the DVR points and the transformation matrix are simply the eigenvalues and the eigenvector matrix of the coordinate operator matrix. We have compared the two DVR schemes, and the DVR points as well as the transformation matrix T from the two methods are nearly the same. For R and r coordinates, we have used potential optimized DVR.[62] The details of the DVRs will be given in Sec. III. The final Hamiltonian matrix-vector multiplication for even spectroscopic symmetry looks like

$$\begin{pmatrix} H_{00} & H_{01} & 0 & 0 \\ H_{10} & H_{11} & H_{12} & 0 \\ 0 & H_{21} & H_{22} & \ddots \\ 0 & 0 & \ddots & \ddots \end{pmatrix} \begin{pmatrix} \psi_{\Omega=0} \\ \psi_{\Omega=1} \\ \psi_{\Omega=2} \\ \vdots \end{pmatrix} = \begin{pmatrix} \phi_{\Omega=0} \\ \phi_{\Omega=1} \\ \phi_{\Omega=2} \\ \vdots \end{pmatrix}, \tag{8}$$

which is a very sparse and large tridiagonal block matrix. For odd spectroscopic symmetry, the Hamiltonian matrix is the same except $\Omega=1,2,...,J$. The spectroscopic symmetry parity is defined as $(-1)^{J+p}$, with p being the parity of the wave function under inversion of the space fixed nuclear coordinates. We calculate at the outset and then store the neighboring Coriolis coupling matrices [see the last two terms in Eq. (7) for the details of the matrix elements] for each Ω component. The memory requirement for the coupling matrices is not large, and whenever they are needed in the iterations, we use them to perform the Hamiltonian matrix vector multiplications directly within the DVR. Although it is implemented as a single matrix multiply, the Coriolis coupling matrix multiplication onto the coupling wave packet $\psi_{\Omega\pm1}$ can be interpreted as first transforming the DVR wave packets $\psi_{\Omega\pm1}$ into the FBR, then acting with the Coriolis operator in the FBR, and finally transforming back into the (Ω-dependent) DVR.

B. Lanczos homogeneous filter diagonalization

After setting up Hamiltonian matrix, we use complex symmetric Lanczos algorithm to generate the Lanczos subspace, and then perform LHFD inside the subspace to extract the bound and resonance information for chosen energy windows. The LHFD algorithm for characterizing bound states as well as resonances can be summarized as follows:

(i) Choose a normalized, randomly generated initial vector $\nu_1\neq0$ and set $\beta_1=0$ and $\nu_0=0$. Then use the three-term Lanczos algorithm for complex-symmetric matrices[63]

$$\beta_{k+1}\nu_{k+1}=\hat{H}'\nu_k-\alpha_k\nu_k-\beta_k\nu_{k-1} \tag{9}$$

to project the non-Hermitian absorbing potential augmented Hamiltonian into a Krylov subspace. The $M\times M$ tridiagonal representation of the Hamiltonian, T_M, has diagonal elements $\alpha_k=(\nu_k|\hat{H}'|\nu_k)$ and subdiagonal elements $\beta_k=(\nu_{k-1}|\hat{H}'|\nu_k)$. Note that a complex-symmetric inner product is used (i.e., bra vectors are not complex conjugated).

(ii) For all $j=1,2,...,j_{\max}$, generate filtered states $\phi(E_j)$ by solving the homogeneous linear system

$$(E_j-T_M)|\phi(E_j)\rangle=0. \tag{10}$$

Here a backward substitution recursion is employed: Choose ϕ_M, the Mth element of $\phi(E_j)$, to be arbitrary (but nonzero; usually set $\phi_M=1$), and calculate

$$\phi_{M-1}=\frac{1}{\beta_M}(E_j\phi_M-\alpha_M\phi_M). \tag{11}$$

For $k=M-1,M-2,...,2$, update scalar ϕ_{k-1}:

$$\beta_k\phi_{k-1}=E_j\phi_k-\alpha_k\phi_k-\beta_{k+1}\phi_{k+1}. \tag{12}$$

(iii) Construct the overlap matrix with elements $S_{jj'}=(\phi(E_j)|\phi(E_{j'}))$ and subspace Hamiltonian matrix with elements $W_{jj'}=(\phi(E_j)|T_M|\phi(E_{j'}))$. Note that $W_{jj'}$ can be calculated using a three-term summation:

$$W_{jj'}=\sum_{k=1}^{M}[\phi_k(E_j)\beta_k\phi_{k-1}(E_{j'})+\phi_k(E_j)\alpha_k\phi_k(E_{j'}) + \phi_k(E_j)\beta_{k+1}\phi_{k+1}(E_{j'})]. \tag{13}$$

(iv) Solve the generalized complex-symmetric eigenvalue problem $WB=SB\varepsilon$ to obtain the complex energies, $\{\varepsilon\}$.

(v) Span the energy domain by repeating (ii)–(iv) window by window.

To check the convergence of the eigenvalues as well as the quality of the eigenpairs generated by the above iterative methods, one can typically compute the error norm about the eigenenergy E,

$$\sigma(E)=\|(T_M-E)\zeta(E)\| \tag{14}$$

where the Lanczos eigenvector $\zeta(E)$ is cheaply regenerated for each complex eigenenergy using Eq. (10). Clearly, true eigenvalues should have small error norms and can thus be distinguished from any unconverged/spurious eigenvalues.

III. RESULTS

A. Calculational details

The triatomic HO_2 Hamiltonian matrix was set up in terms of reactant Jacobi coordinates, and the HO_2 DMBE IV PES[64] was employed as we did for $J=0$ bound and resonance calculations. For the two radial coordinates, a potential-optimized discrete variable representation[62]

TABLE I. Selected low lying bound state energies in energy window 1 for $J=1$ and even spectroscopic symmetry. The results of Wu and Hayes (Ref. 34) are also included for comparison. LHFD indicates this work, and Ω indicates the helicity quantum number assignment. $^+$ means even spectroscopic symmetry and $^-$ means odd spectroscopic symmetry. The rovibrational ground state energy was calculated at $-2.015\,861$ eV relative to the dissociation limit of $H+O_2$, which is referred to as the zero energy point. All energy units are in eV.

n	LHFD	Ref. 34	Ω	n	LHFD	Ref. 34	Ω
1	0.000 271	0.000 270	0^+	18	0.422 581	0.422 618	1^+
2	0.002 668	0.002 668	1^+	19	0.445 320	0.445 347	0^+
3	0.132 352	0.132 368	0^+	20	0.447 875	0.447 903	1^+
4	0.134 720	0.134 736	1^+	21	0.462 197	0.462 211	0^+
5	0.160 996	0.161 003	0^+	22	0.464 906	0.464 921	1^+
6	0.163 488	0.163 496	1^+	23	0.501 247	0.501 304	0^+
7	0.259 495	0.259 525	0^+	24	0.503 535	0.503 592	1^+
8	0.261 834	0.261 865	1^+	25	0.541 845	0.541 891	0^+
9	0.292 789	0.292 812	0^+	26	0.544 223	0.544 269	1^+
10	0.295 249	0.295 272	1^+	27	0.548 433	0.548 455	0^+
11	0.312 291	0.312 302	0^+	28	0.550 718	0.550 741	1^+
12	0.314 886	0.314 898	1^+	29	0.572 484	0.572 523	0^+
13	0.382 208	0.382 252	0^+	30	0.574 994	0.575 033	1^+
14	0.384 520	0.384 564	1^+	31	0.581 538	0.581 552	0^+
15	0.413 593	0.413 598	0^+	32	0.583 961	0.583 976	1^+
16	0.415 892	0.415 896	1^+	33	0.597 478	0.597 507	0^+
17	0.420 161	0.420 197	0^+	34	0.600 120	0.600 151	1^+

TABLE II. Selected low bound state energies from energy window 1 from $J=1$ and odd spectroscopic symmetry calculations. All other symbols are the same as in Table I.

n	LHFD	Ref. 34	Ω	n	LHFD	Ref. 34	Ω
1	0.002 675	0.002 675	1^-	9	0.422 589	0.422 627	1^-
2	0.134 728	0.134 744	1^-	10	0.447 884	0.447 912	1^-
3	0.163 496	0.163 505	1^-	11	0.464 913	0.464 931	1^-
4	0.261 842	0.261 872	1^-	12	0.503 543	0.503 600	1^-
5	0.295 257	0.295 281	1^-	13	0.544 231	0.544 278	1^-
6	0.314 893	0.314 907	1^-	14	0.550 726	0.550 749	1^-
7	0.384 527	0.384 572	1^-	15	0.575 002	0.575 043	1^-
8	0.415 902	0.415 904	1^-	16	0.583 969	0.583 985	1^-

(PODVR) was utilized to reduce the size of the Hamiltonian matrix. For the R coordinate, we have used $N_R=110$ PODVR points, which were contracted from 315 evenly-spaced primitive sinc DVR points[65] spanning the range from 0.5 a_0 to 11.0 a_0 with the one-dimensional reference potential $V(R,r_e,\theta_e)$. Similarly, for the r coordinate, $N_r=50$ PODVR points were obtained from 150 primary DVR points spanning the range from 1.3 a_0 to 5.0 a_0 using the reference potential $V(R_e,r,\theta_e)$. For the γ variable, Ω-dependent symmetry-adapted DVR functions, defined by corresponding associated Gauss–Legendre quadrature points, were employed to take account of the odd O–O exchange parity. Another kind of symmetry originated from the Wigner D-functions, i.e., spectroscopic symmetry, has also been considered. The resulting direct product basis set was further contracted by discarding those points whose potential energies were higher than the cutoff energy $V_{\text{cutoff}}=2.0$ eV, resulting in the final basis size of $110\,700\times(J+1)$ for even spectroscopic symmetry and $110\,700\times J$ for odd spectroscopic symmetry.

For the LHFD calculations, the absorbing potential in the dissociation channel of $H+O_2$ takes the following form:

$$\hat{V}_{abs}(R)=\frac{V_0}{\cosh^2[(R_{\max}-R)/\lambda]}, \tag{15}$$

TABLE III. Selected low bound state energies from energy window 1 from $J=2$ and even spectroscopic symmetry calculations. Other symbols are the same as in Table I.

n	LHFD	Ref. 34	Ω	n	LHFD	Ref. 34	Ω
1	0.000 811	0.000 811	0^+	16	0.312 835	0.312 848	0^+
2	0.003 200	0.003 201	1^+	17	0.315 425	0.315 434	1^+
3	0.010 408	0.010 410	2^+	18	0.323 229	0.323 241	2^+
4	0.132 881	0.132 897	0^+	19	0.382 714	0.382 758	0^+
5	0.135 241	0.135 257	1^+	20	0.385 019	0.385 063	1^+
6	0.142 362	0.142 379	2^+	21	0.391 974	0.392 019	2^+
7	0.161 540	0.161 547	0^+	22	0.414 139	0.414 142	0^+
8	0.164 025	0.164 031	1^+	23	0.416 425	0.416 432	1^+
9	0.171 520	0.171 528	2^+	24	0.420 681	0.420 718	2^+
10	0.260 012	0.260 043	0^+	25	0.423 094	0.423 130	0^+
11	0.262 343	0.262 374	1^+	26	0.423 336	0.423 344	1^+
12	0.269 379	0.269 410	2^+	27	0.430 377	0.430 414	2^+
13	0.293 321	0.293 344	0^+	28	0.445 853	0.445 880	0^+
14	0.295 772	0.295 795	1^+	29	0.448 401	0.448 427	1^+
15	0.303 170	0.303 194	2^+	30	0.456 087	0.456 115	2^+

TABLE IV. Selected low bound state energies from energy window 1 from $J=2$ and odd spectroscopic symmetry calculations. Other symbols are the same as in Table I.

n	LHFD	Ref. 34	Ω	n	LHFD	Ref. 34	Ω
1	0.003 224	0.003 224	1^-	11	0.315 450	0.315 462	1^-
2	0.010 408	0.010 410	2^-	12	0.323 228	0.323 241	2^-
3	0.135 264	0.135 280	1^-	13	0.385 041	0.385 086	1^-
4	0.142 362	0.142 379	2^-	14	0.391 974	0.392 019	2^-
5	0.164 049	0.164 057	1^-	15	0.416 453	0.416 456	1^-
6	0.171 519	0.171 528	2^-	16	0.423 119	0.423 156	2^-
7	0.262 366	0.262 397	1^-	17	0.423 337	0.423 344	1^-
8	0.269 379	0.269 410	2^-	18	0.430 377	0.430 414	2^-
9	0.295 798	0.295 821	1^-	19	0.448 428	0.448 456	1^-
10	0.303 170	0.303 194	2^-	20	0.456 087	0.456 115	2^-

where $R_{\max}=11.0\,a_0$, and V_0 and λ are two adjusting parameters. For our purposes we take $V_0=2.0$ eV and $\lambda=0.5\,a_0$.

B. Bound and resonance energies

We have employed the LHFD methods described in detail above to compute the bound state energies as well as the resonance energies and widths for two chosen energy windows for low J values 1, 2, 3. The first energy window is for the lowest bound state energies from -0.08 eV to 0.92 eV. Here the zero energy point is referred to as the ground state energy of HO_2 for $J=0$, which is $-2.015\,861$ eV relative to the $H+O_2$ dissociation limit. For this energy window we can also compare our results with the early calculated results from Wu and Hayes.[34] This energy window is relatively easy to calculate and a Lanczos subspace size $M=5000$ is enough to converge all the energies in this window. In Tables I–VI we have listed the bound state energies for each symmetry of $J=1$, 2, and 3 separately. Inspection of the energies shows that the agreement between our results and the earlier ones are quite satisfactory and four digits of relative accuracy has been achieved for most of the energies.

The second energy window we have chosen is close to and above dissociation threshold, namely, the highest lying bound state energies and lowest resonance energies and widths from 2.10 eV to 2.18 eV. Since these are the first

TABLE V. Selected low bound state energies from energy window 1 from $J=3$ and even spectroscopic symmetry calculations. Other symbols are the same as in Table I.

n	LHFD	Ref. 34	Ω	n	LHFD	Ref. 34	Ω
1	0.001 622	0.001 623	0^+	15	0.270 154	0.270 186	2^+
2	0.004 000	0.004 000	1^+	16	0.281 844	0.281 877	3^+
3	0.011 219	0.011 221	2^+	17	0.294 119	0.294 142	0^+
4	0.023 195	0.023 198	3^+	18	0.296 557	0.296 580	1^+
5	0.133 674	0.133 690	0^+	19	0.303 967	0.303 992	2^+
6	0.136 023	0.136 039	1^+	20	0.313 655	0.313 667	3^+
7	0.143 155	0.143 172	2^+	21	0.316 228	0.316 240	0^+
8	0.154 986	0.155 005	3^+	22	0.316 253	0.316 279	1^+
9	0.162 356	0.162 363	0^+	23	0.324 047	0.324 060	2^+
10	0.164 827	0.164 834	1^+	24	0.337 002	0.337 018	3^+
11	0.172 335	0.172 344	2^+	25	0.383 474	0.383 518	0^+
12	0.184 783	0.184 793	3^+	26	0.385 767	0.385 812	1^+
13	0.260 788	0.260 819	0^+	27	0.392 733	0.392 778	2^+
14	0.263 108	0.263 139	1^+	28	0.404 289	0.404 336	3^+

TABLE VI. Selected low bound state energies from energy window 1 from $J=3$ and odd spectroscopic symmetry calculations. Other symbols are the same as in Table I.

n	LHFD	Ref. 34	Ω	n	LHFD	Ref. 34	Ω
1	0.004 046	0.004 047	1^-	9	0.184 783	0.184 793	3^-
2	0.011 219	0.011 221	2^-	10	0.263 154	0.263 185	1^-
3	0.023 195	0.023 198	3^-	11	0.270 154	0.270 186	2^-
4	0.136 069	0.136 085	1^-	12	0.281 844	0.281 877	3^-
5	0.143 155	0.143 172	2^-	13	0.296 609	0.296 632	1^-
6	0.154 986	0.155 005	3^-	14	0.303 967	0.303 992	2^-
7	0.164 878	0.164 886	1^-	15	0.316 253	0.316 279	3^-
8	0.172 334	0.172 344	2^-	16	0.316 284	0.316 296	1^-

calculated results, the convergence has been carefully tested and in Fig. 1 we have plotted the convergence behavior for one resonance at $E=2.133\,96$ eV for $J=1$ (odd symmetry). From this figure one can see that $M=100\,000$ Lanczos iterations can well converge most of the resonances in this energy rage and in all our calculations we have used a larger $M=150\,000$ Lanczos subspace size. In Tables VII–XII we present the resonance energies and widths for each symmetry of $J=1$, 2, and 3, respectively. These resonances are relatively narrow ones and broader resonances cannot be extracted from the spectrum, simply because they are hidden in the background. Also we do not attempt to perform stabilization calculations for each resonance due to too large demanding on the computational resources.

Analysis of the resonance widths shows that most of the resonances are overlapping ones. In Fig. 2 we have plotted the resonance widths versus energies for $J=1$, 2, 3 (resonances from both even and odd symmetries are put together). Our considered energy range is relative small, but the fluctuations from the three figures are not small at all. It seems that the quantum widths (related to unimolecular dissociation rates) fluctuate from one resonance to another in a random and an unpredictable way. Such a fluctuation is a manifestation of prominent quantum interference effects between overlapping resonances. This fluctuating behavior has also been obtained from $J=0$ theoretical calculations on HO_2 dissociation by several groups,[13,26,31] which indicates that the dissociation of HO_2 is essentially irregular. Although experimental data are still not available for this system, fluctuating resonance rates have been observed for several other dissociation systems including H_2CO, CH_3O, and NO_2.[66–68]

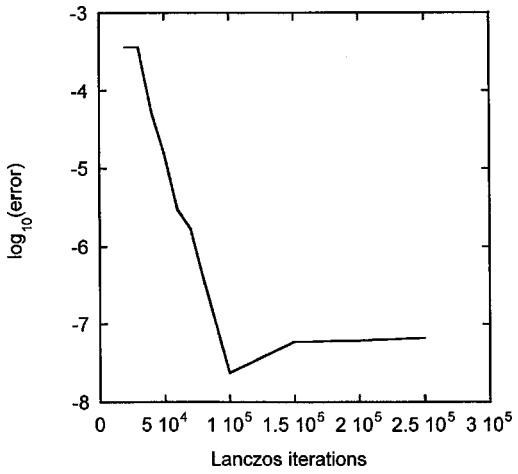

FIG. 1. Plot of the logarithmic relative errors, $\log_{10}$(error), versus Lanczos iteration sizes at one resonance energy $E=2.133\,96$ eV from $J=1$ odd symmetry calculations. All errors are relative to the reference energy of $E=2.133\,957\,694\,6$ eV from the largest subspace size $M=300\,000$ calculations.

TABLE VII. Selected resonance energies and widths from energy window 2 from $J=1$ and even spectroscopic symmetry calculations. All results are from this work. The resonance energies are relative to the ro-vibrational ground state energy of 2.015 861 eV from $J=0$ calculations. All energy units are in eV.

n	Energy (LHFD)	Width (LHFD)	n	Energy (LHFD)	Width (LHFD)
1	2.115 615	$0.96E-04$	15	2.123 716	$0.87E-05$
2	2.115 940	$0.21E-04$	16	2.124 557	$0.75E-04$
3	2.116 007	$0.50E-04$	17	2.125 397	$0.11E-04$
4	2.117 532	$0.72E-04$	18	2.126 727	$0.66E-03$
5	2.117 632	$0.18E-03$	19	2.127 894	$0.83E-04$
6	2.118 151	$0.15E-06$	20	2.129 499	$0.14E-02$
7	2.118 766	$0.11E-03$	21	2.129 565	$0.20E-05$
8	2.119 246	$0.79E-04$	22	2.130 381	$0.34E-05$
9	2.120 072	$0.55E-03$	23	2.130 942	$0.34E-04$
10	2.120 213	$0.16E-04$	24	2.131 559	$0.27E-03$
11	2.121 811	$0.60E-04$	25	2.132 133	$0.90E-03$
12	2.121 944	$0.41E-03$	26	2.133 084	$0.13E-04$
13	2.122 115	$0.25E-03$	27	2.133 194	$0.34E-04$
14	2.123 205	$0.89E-06$	28	2.134 299	$0.13E-03$

Finally, in Tables I–VI an unambiguous Ω assignment has been given for the low-lying bound states, supposing that the helicity conserving approximation holds (because there exist near degeneracies for the same Ω components from both symmetries, it is possible to assign them by comparing the calculated energies from even and odd symmetries). The purpose of Ω assignment is to investigate the importance of the Coriolis coupling for this system. If this assignment is successful, then helicity conserving (HC) calculations should be accurate, which will save quite a lot of computational time. For the high-lying bound states as well as for the resonances, we have failed to assign them unambiguously. For example, we have analyzed the high-lying bound state energies near the dissociation threshold from $J=1$ calculations for both even and odd spectroscopic symmetries, respec-

TABLE VIII. Selected resonance energies and widths from energy window 2 from $J=1$ and odd spectroscopic symmetry calculations. Other symbols are the same as in Table VII.

n	Energy (LHFD)	Width (LHFD)	n	Energy (LHFD)	Width (LHFD)
1	2.115 124	$0.37E-04$	9	2.124 787	$0.33E-03$
2	2.116 654	$0.14E-03$	10	2.125 180	$0.11E-03$
3	2.118 201	$0.89E-04$	11	2.126 976	$0.54E-03$
4	2.119 989	$0.37E-03$	12	2.127 957	$0.43E-03$
5	2.120 155	$0.10E-03$	13	2.130 496	$0.23E-03$
6	2.120 639	$0.38E-03$	14	2.132 355	$0.18E-03$
7	2.121 335	$0.35E-03$	15	2.133 304	$0.18E-02$
8	2.123 094	$0.13E-03$	16	2.133 958	$0.16E-04$

TABLE IX. Selected resonance energies and widths from energy window 2 from $J=2$ and even spectroscopic symmetry calculations. Other symbols are the same as in Table VII.

n	Energy (LHFD)	Width (LHFD)	n	Energy (LHFD)	Width (LHFD)
1	2.115 111	$0.65E-05$	21	2.123 966	$0.80E-03$
2	2.115 438	$0.17E-04$	22	2.124 270	$0.24E-04$
3	2.115 799	$0.99E-05$	23	2.125 191	$0.10E-03$
4	2.116 490	$0.20E-04$	24	2.125 260	$0.88E-04$
5	2.116 649	$0.33E-05$	25	2.125 840	$0.57E-03$
6	2.117 014	$0.44E-03$	26	2.126 601	$0.22E-03$
7	2.117 971	$0.31E-03$	27	2.126 638	$0.47E-03$
8	2.118 494	$0.54E-04$	28	2.126 871	$0.66E-04$
9	2.118 581	$0.92E-04$	29	2.126 889	$0.41E-03$
10	2.118 964	$0.38E-04$	30	2.127 681	$0.38E-04$
11	2.119 042	$0.83E-03$	31	2.128 527	$0.37E-03$
12	2.119 276	$0.16E-03$	32	2.129 272	$0.15E-04$
13	2.120 353	$0.21E-04$	33	2.129 329	$0.12E-04$
14	2.120 670	$0.37E-04$	34	2.130 435	$0.92E-04$
15	2.121 447	$0.62E-04$	35	2.130 675	$0.36E-04$
16	2.121 541	$0.11E-03$	36	2.131 177	$0.44E-04$
17	2.121 696	$0.28E-04$	37	2.131 484	$0.10E-03$
18	2.123 237	$0.22E-04$	38	2.131 530	$0.13E-04$
19	2.123 409	$0.16E-03$	39	2.131 838	$0.15E-02$
20	2.123 660	$0.51E-04$	40	2.132 128	$0.18E-05$

TABLE XI. Selected resonance energies and widths from energy window 2 from $J=3$ and even spectroscopic symmetry calculations. Other symbols are the same as in Table VII.

n	Energy (LHFD)	Width (LHFD)	n	Energy (LHFD)	Width (LHFD)
1	2.114 890	$0.21E-04$	21	2.123 500	$0.40E-03$
2	2.115 157	$0.16E-04$	22	2.124 398	$0.13E-04$
3	2.116 115	$0.28E-06$	23	2.125 038	$0.61E-05$
4	2.116 582	$0.68E-05$	24	2.125 702	$0.27E-03$
5	2.116 830	$0.42E-04$	25	2.126 171	$0.99E-04$
6	2.117 415	$0.17E-04$	26	2.126 612	$0.65E-04$
7	2.117 513	$0.13E-03$	27	2.127 339	$0.34E-04$
8	2.117 638	$0.23E-03$	28	2.127 699	$0.46E-05$
9	2.117 936	$0.56E-03$	29	2.128 075	$0.21E-04$
10	2.118 330	$0.57E-04$	30	2.128 473	$0.12E-02$
11	2.118 967	$0.78E-04$	31	2.129 215	$0.14E-03$
12	2.119 048	$0.15E-04$	32	2.129 751	$0.23E-03$
13	2.119 506	$0.10E-02$	33	2.130 537	$0.88E-03$
14	2.119 829	$0.94E-04$	34	2.130 736	$0.67E-04$
15	2.120 150	$0.52E-04$	35	2.131 283	$0.14E-04$
16	2.121 257	$0.59E-04$	36	2.132 044	$0.33E-04$
17	2.121 417	$0.56E-04$	37	2.132 124	$0.65E-04$
18	2.122 265	$0.42E-03$	38	2.132 497	$0.39E-03$
19	2.122 916	$0.32E-03$	39	2.133 296	$0.15E-02$
20	2.123 335	$0.17E-03$	40	2.134 151	$0.17E-04$

tively. (The results for the high-lying bound state energies are not shown here, and they can be acquired from us upon request.) While only several of them from $J=1$ even symmetry calculations can be assigned tentatively, most of them cannot be assigned with confidence (for $J=1$ odd symmetry results there is no need to assign because only one component $\Omega=1$ exists). The indication is that the mixing of different Ω components is so strong for them that Ω is no longer a good quantum number. Of course, the difficulties in assignment also arise from the fact that the spacings between these high-lying bound states and resonance states are becoming smaller and smaller. For overlapping resonances, the assignment is further complicated by the mixing of different resonance states, i.e., at resonance energy, other neighboring resonances might interfere with this ''main'' resonance. For this system, it seems that HC calculations can give reasonably accurate results only for low bound state energies. This observation is in consistent with the previously reported $J>0$ total reaction probability calculations for this system, which show that for HO_2 the Coriolis coupling is important and cannot be ignored.[69] Interestingly, this situation is in contrast to the H_2O system, for which HC calculations can predict quite accurate total reaction probabilities.[70,71]

TABLE X. Selected resonance energies and widths from energy window 2 from $J=2$ and odd spectroscopic symmetry calculations. Other symbols are the same as in Table VII.

n	Energy (LHFD)	Width (LHFD)	n	Energy (LHFD)	Width (LHFD)
1	2.114 868	$0.11E-05$	16	2.124 291	$0.18E-04$
2	2.115 574	$0.53E-05$	17	2.124 380	$0.40E-03$
3	2.116 195	$0.25E-05$	18	2.125 595	$0.10E-02$
4	2.116 429	$0.15E-04$	19	2.125 853	$0.20E-04$
5	2.116 728	$0.54E-04$	20	2.126 950	$0.93E-04$
6	2.117 200	$0.64E-03$	21	2.127 115	$0.18E-01$
7	2.117 740	$0.61E-04$	22	2.127 474	$0.65E-03$
8	2.118 729	$0.91E-04$	23	2.128 793	$0.83E-04$
9	2.119 612	$0.78E-04$	24	2.130 450	$0.72E-03$
10	2.120 857	$0.11E-03$	25	2.130 836	$0.77E-05$
11	2.121 512	$0.32E-03$	26	2.131 321	$0.43E-05$
12	2.121 778	$0.10E-02$	27	2.132 097	$0.43E-03$
13	2.122 184	$0.40E-03$	28	2.132 892	$0.15E-02$
14	2.122 643	$0.61E-05$	29	2.133 648	$0.83E-05$
15	2.124 159	$0.34E-03$	30	2.134 665	$0.16E-04$

TABLE XII. Selected resonance energies and widths from energy window 2 from $J=3$ and odd spectroscopic symmetry calculations. Other symbols are the same as in Table VII.

n	Energy (LHFD)	Width (LHFD)	n	Energy (LHFD)	Width (LHFD)
1	2.114 837	$0.48E-05$	19	2.124 190	$0.17E-04$
2	2.115 698	$0.18E-05$	20	2.124 864	$0.94E-04$
3	2.116 131	$0.91E-05$	21	2.125 135	$0.17E-04$
4	2.116 308	$0.22E-05$	22	2.126 286	$0.79E-04$
5	2.117 299	$0.17E-06$	23	2.126 588	$0.21E-03$
6	2.118 239	$0.25E-03$	24	2.127 464	$0.46E-04$
7	2.118 494	$0.40E-03$	25	2.127 961	$0.39E-05$
8	2.118 646	$0.96E-05$	26	2.128 120	$0.51E-03$
9	2.119 368	$0.13E-03$	27	2.128 637	$0.75E-07$
10	2.119 731	$0.16E-03$	28	2.129 578	$0.59E-03$
11	2.120 174	$0.62E-04$	29	2.130 126	$0.45E-04$
12	2.121 093	$0.82E-03$	30	2.130 932	$0.12E-03$
13	2.121 352	$0.19E-04$	31	2.131 309	$0.11E-03$
14	2.121 626	$0.54E-03$	32	2.131 807	$0.53E-04$
15	2.121 946	$0.35E-03$	33	2.132 399	$0.34E-04$
16	2.122 469	$0.50E-05$	34	2.133 563	$0.39E-04$
17	2.123 365	$0.98E-03$	35	2.133 686	$0.55E-04$
18	2.123 570	$0.30E-03$	36	2.133 876	$0.12E-04$

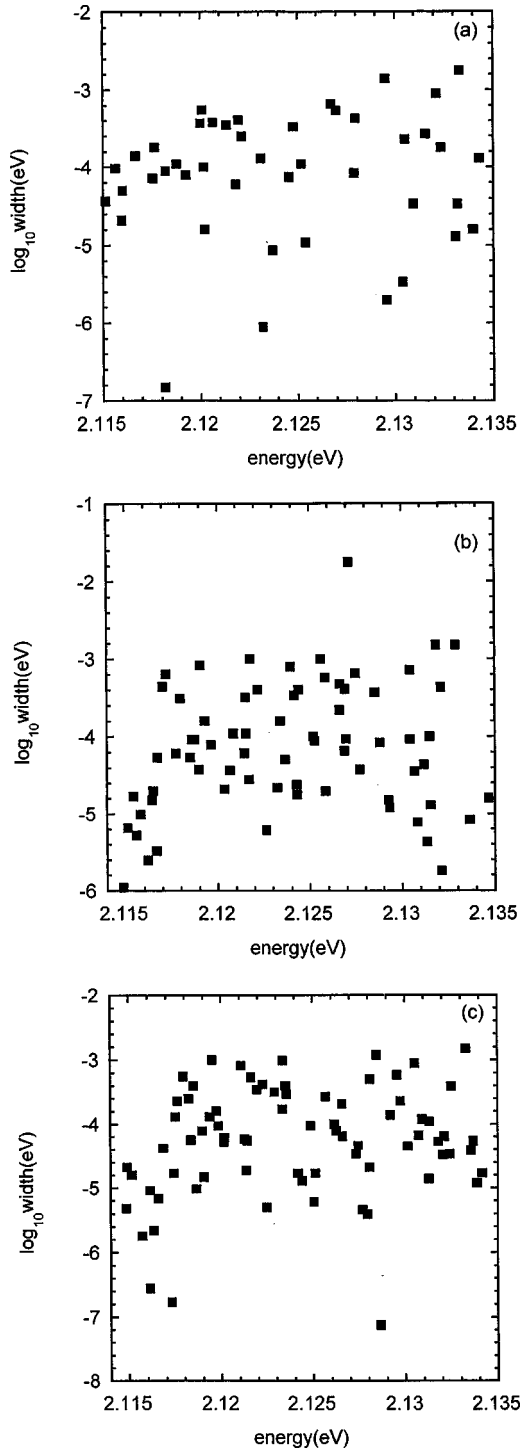

FIG. 2. (a) Plot of the logarithmic resonance widths, $\log_{10}$ (width), versus resonance energy in the low part of the resonance energies from $J=1$ calculations. Resonances from both odd symmetry and even symmetry have been included. (b) Same as previous figure, except from $J=2$ calculations. (c) Same as previous figure, except from $J=3$ calculations.

IV. CONCLUSIONS

In this paper the Lanszos subspace FD method developed in this group has been successfully extended to $J>0$ calculations and converged HO_2 bound state energies as well as resonance energies and widths have been obtained for low J values 1, 2, and 3. For low-lying bound states, agreement between our results and the earlier calculations of Wu and Hayes is quite satisfactory. For higher-lying bound states and resonances, these are the first reported results. The results indicate that the unimolecular dissociation of HO_2 is dominated by numerous resonances starting just above dissociation threshold for $J>0$. Most of these resonances are overlapping ones, and the interferences among them lead to complicated dissociation dynamics. The resonance widths (rates) show strong fluctuations, which indicate there is an intricate coupling between the internal degrees of freedom in dissociation, and that the HO_2 dissociation is essentially irregular.

An Ω assignment has been attempted to investigate the importance of the Coriolis coupling. While this assignment is successful for the low bound states, for the higher-lying bound states and resonances the assignment is unsuccessful. This indicates that mixing of different Ω components is strong and Coriolis coupling cannot be ignored for this system (Ω *is no longer a good quantum number*), especially for resonance calculations.

Several interesting issues concerning HO_2 dissociation suggest themselves for future work and are under investigation in our group. First, inspired by the work of Goldfield and co-workers,[39–41] we are extending our $J>0$ bound and resonance calculations to high J values through parallel computing. We are also performing a comparative study of the Lanczos subspace FD method with the real Chebyshev FD method[72] for J values ranging 1 through 5 and the preliminary results are encouraging.[73] In addition, it will be interesting to compare the r-embedding resonances (O–O bond as the z axis of the body-fixed frame) with the R-embedding results of this paper, since it has been suggested that the r axis may be a better quantization axis (in the sense of preserving Ω as a good quantum number). For the reactive scattering case, such a comparison has been made to investigate the importance of the Coriolis coupling.[41] In that study, it was found that Ω is not a good quantum number for either embedding, however, whether this conclusion also holds for high-lying bound states and resonances remains to be seen. Finally we are implementing the pseudo-spectral transformation representation into our algorithms for efficiently implementing the Hamiltonian matrix vector multiplications (see, e.g., Refs. 51, 52), which is essential in all iterative quantum methods and in particular for $J>0$ calculations.

ACKNOWLEDGMENTS

We are grateful to the Australian Research Council for supporting this work (Large Grant No. A29937112 and Discovery Project Grant No. DP0211019). We thank Dr. Anthony Rasmussen and Dr. Hua-Gen Yu for helpful discussions. We also acknowledge the grants of high performance computer time from both The University of Queensland and the Australian Partnership for Advanced Computing (APAC) National facility.

[1] G. Jolicard, C. Leforestier, and E. J. Austin, J. Chem. Phys. **88**, 1026 (1988).
[2] G. Jolicard and E. J. Austin, Chem. Phys. Lett. **121**, 106 (1985).
[3] G. Jolicard and E. J. Austin, Chem. Phys. **103**, 295 (1986).
[4] D. Neuhauser and M. Baer, J. Chem. Phys. **90**, 4351 (1989).
[5] R. Kosloff and D. Kosloff, J. Comput. Phys. **63**, 363 (1986).

[6] U. V. Riss and H.-D. Meyer, J. Phys. B **26**, 4503 (1993).
[7] J. Aguilar and J. M. Combes, Commun. Math. Phys. **22**, 269 (1971).
[8] B. Simon, Ann. Math. **97**, 247 (1973).
[9] N. Moiseyev, P. R. Certain, and F. Weinhold, Mol. Phys. **36**, 1613 (1978).
[10] N. Moiseyev, Phys. Rep. **302**, 211 (1998).
[11] K. T. Lee and J. M. Bowman, J. Chem. Phys. **85**, 6225 (1986).
[12] H. W. Jang and J. C. Light, J. Chem. Phys. **102**, 3262 (1995).
[13] A. J. Dobbyn, M. Stumpf, H.-M. Keller, and R. Schinke, J. Chem. Phys. **104**, 8357 (1996).
[14] R. Schinke, H.-M. Keller, M. Stumpf, and A. J. Dobbyn, J. Phys. B **28**, 3081 (1995).
[15] M. Stumpf, A. J. Dobbyn, D. H. Mordaunt, H.-M. Keller, H. Fluethmann, and R. Schinke, Faraday Discuss. **102**, 193 (1995).
[16] F. Fernandez-Alonso and R. N. Zare, Annu. Rev. Phys. Chem. **53**, 67 (2002).
[17] K. Liu, Annu. Rev. Phys. Chem. **52**, 139 (2001).
[18] S. A. Reid and H. Reisler, Annu. Rev. Phys. Chem. **47**, 495 (1996).
[19] R. Schinke, H.-M. Keller, H. Flothmann, M. Stumpf, C. Beck, D. H. Mordaunt, and A. J. Dobbyn, Adv. Chem. Phys. **101**, 745 (1997).
[20] J. M. Bowman, J. Phys. Chem. A **102**, 3006 (1998).
[21] R. Schinke, C. Beck, S. Y. Grebenshchikov, and H. M. Keller, Ber. Bunsenges. Phys. Chem. **102**, 593 (1998).
[22] W. H. Miller, Annu. Rev. Phys. Chem. **41**, 245 (1990).
[23] G. C. Schatz, Science **288**, 1599–1600 (2000).
[24] H. Zhang and S. C. Smith, Phys. Chem. Chem. Phys. **3**, 2282 (2001).
[25] H. Zhang and S. C. Smith, J. Chem. Phys. **115**, 5751 (2001).
[26] V. A. Mandelshtam, T. P. Grozdanov, and H. S. Taylor, J. Chem. Phys. **103**, 10074 (1995).
[27] B. Kendrick and R. T Pack, Chem. Phys. Lett. **235**, 291 (1995).
[28] B. Kendrick and R. T Pack, J. Chem. Phys. **104**, 7475 (1996).
[29] J. Dai and J. Z. H. Zhang, J. Phys. Chem. **100**, 6899 (1996).
[30] D. H. Zhang and J. Z. H. Zhang, J. Chem. Phys. **101**, 3671 (1994).
[31] A. J. Dobbyn, M. Stumpf, H.-M. Keller, W. L. Hase, and R. Schinke, J. Chem. Phys. **102**, 5867 (1995).
[32] H. Zhang and S. C. Smith, Chem. Phys. Lett. **347**, 211 (2001).
[33] H. G. Yu and S. C. Smith, Chem. Phys. Lett. **283**, 69 (1998).
[34] X. T. Wu and E. F. Hayes, J. Chem. Phys. **107**, 2705 (1997).
[35] C. Leforestier and W. H. Miller, J. Chem. Phys. **100**, 733 (1994).
[36] J. Q. Dai and J. Z. H. Zhang, J. Chem. Phys. **104**, 3664 (1996).
[37] R. T Pack, E. A. Butcher, and G. A. Parker, J. Chem. Phys. **99**, 9310 (1993).
[38] R. T Pack, E. A. Butcher, and G. A. Parker, J. Chem. Phys. **102**, 5998 (1995).
[39] E. M. Goldfield and A. J. H. M. Meijer, J. Chem. Phys. **113**, 11055 (2000).
[40] A. Meijer and E. M. Goldfield, J. Chem. Phys. **108**, 5404 (1998).
[41] A. Meijer and E. M. Goldfield, J. Chem. Phys. **110**, 870 (1999).
[42] H. Zhang and S. C. Smith, J. Chem. Phys. **116**, 2354 (2002).
[43] H. Zhang and S. C. Smith, J. Chem. Phys. **117**, 5174 (2002).
[44] W. C. Gardiner, *Combustion Chemistry* (Springer, Berlin, 1984).
[45] D. G. Truhlar, Comput. Phys. Commun. **84**, 78 (1994).
[46] J. M. Bowman, Chem. Phys. Lett. **217**, 36 (1993).
[47] J. M. Bowman, J. Phys. Chem. **95**, 4960 (1991).
[48] D. E. Skinner, T. C. German, and W. H. Miller, J. Phys. Chem. A **102**, 3828 (1998).
[49] R. C. Mowrey and D. J. Kouri, J. Chem. Phys. **84**, 6466 (1986).
[50] J. C. Light, I. P. Hamilton, and J. V. Lill, J. Chem. Phys. **82**, 1400 (1985).
[51] G. Corey and D. Lemoine, J. Chem. Phys. **97**, 4115 (1992).
[52] A. J. Rasmussen, K. E. Gates, and S. C. Smith, J. Chem. Phys. **110**, 1354 (1999).
[53] C. Lanczos, J. Res. Natl. Bur. Stand. **45**, 255 (1950).
[54] J. K. Cullum and R. A. Willoughby, *Lanczos Algorithms for Large Symmetric Eigenvalue Computations* (Birkhauser, Boston, 1985).
[55] H. G. Yu and S. C. Smith, Ber. Bunsenges. Phys. Chem. **101**, 400 (1997).
[56] H. G. Yu and S. C. Smith, J. Chem. Phys. **107**, 9985 (1997).
[57] H. G. Yu and S. C. Smith, J. Comput. Phys. **143**, 484 (1998).
[58] S. E. Choi and J. C. Light, J. Chem. Phys. **92**, 2129 (1990).
[59] C. Leforestier, J. Chem. Phys. **94**, 6388 (1991).
[60] S. M. Auerbach and W. H. Miller, J. Chem. Phys. **100**, 1103 (1994).
[61] W. H. Press, S. A. Teukolsky, W. T. Vetterling, and B. P. Flannery, *Numerical Recipes in Fortran* (Cambridge University Press, Cambridge, 1992).
[62] J. Echave and D. Clary, Chem. Phys. Lett. **190**, 225 (1992).
[63] G. Moro and J. H. Freed, J. Chem. Phys. **74**, 3757 (1981).
[64] M. R. Pastrana, L. A. M. Quintales, J. Brandao, and A. J. C. Varandas, J. Phys. Chem. **94**, 8073 (1990).
[65] D. T. Colbert and W. H. Miller, J. Chem. Phys. **96**, 1982 (1992).
[66] A. Geers, J. Kappert, F. Temps, and J. W. Wiebrecht, J. Chem. Phys. **99**, 2271 (1993).
[67] W. H. Miller, R. Hernandez, C. B. Moore, and W. F. Polik, J. Chem. Phys. **93**, 5657 (1990).
[68] S. A. Reid and H. Reisler, J. Phys. Chem. **100**, 474 (1996).
[69] A. J. H. M. Meijer and E. M. Goldfield, Phys. Chem. Chem. Phys. **3**, 2811 (2001).
[70] S. K. Gray, E. M. Goldfield, G. C. Schatz, and G. G. Balint-Kurtii, Phys. Chem. Chem. Phys. **1**, 1141 (1999).
[71] T. E. Carroll and E. M. Goldfield, J. Phys. Chem. A **105**, 2251 (2001).
[72] V. A. Mandelshtam and H. S. Taylor, J. Chem. Phys. **107**, 6756 (1997).
[73] H. Zhang and S. C. Smith, J. Chem. Phys. (to be published).